THE JOURNAL OF BIOLOGICAL CHEMISTRY VOL. 284, NO. 6, pp. 3885–3896, February 6, 2009

The Human Cdc37·Hsp90 Complex Studied by Heteronuclear NMR Spectroscopy*

Received for publication, August 29, 2008, and in revised form, November 18, 2008 Published, JBC Papers in Press, December 10, 2008, DOI 10.1074/jbc.M806715200

Sridhar Sreeramulu[‡], Hendrik R. A. Jonker[‡], Thomas Langer[‡1], Christian Richter[‡], C. Roy D. Lancaster[§¶], and Harald Schwalbe[‡2]

From the [‡]Institute for Organic Chemistry and Chemical Biology, Center for Biomolecular Magnetic Resonance, Johann Wolfgang Goethe-University, Max-von-Laue-Strasse 7, Frankfurt am Main D-60438, the [§]Department of Molecular Membrane Biology, Max Planck Institute of Biophysics, Max-von-Laue-Strasse 3, Frankfurt am Main D-60438, and the [¶]Department of Structural Biology, Saarland University, Faculty of Medicine, Building 60, Homburg D-66421, Germany

The cell division cycle protein 37 (Cdc37) and the 90-kDa heat shock protein (Hsp90) are molecular chaperones, which are crucial elements in the protein signaling pathway. The largest class of client proteins for Cdc37 and Hsp90 are protein kinases. The catalytic domains of these kinases are stabilized by Cdc37, and their proper folding and functioning is dependent on Hsp90. Here, we present the x-ray crystal structure of the 16-kDa middle domain of human Cdc37 at 1.88 Å resolution and the structure of this domain in complex with the 23-kDa N-terminal domain of human Hsp90 based on heteronuclear solution state NMR data and docking. Our results demonstrate that the middle domain of Cdc37 exists as a monomer. NMR and mutagenesis experiments reveal Leu-205 in Cdc37 as a key residue enabling complex formation. These findings can be very useful in the development of small molecule inhibitors against cancer.

The 90-kDa heat shock protein (Hsp90)[3] is an abundant and essential protein, accounting for 1–2% of the total protein amount in unstressed eukaryotic cells. A 2- to 10-fold higher expression level of Hsp90 is found in cancer cells and virally transformed cells (1–3), suggesting a crucial role of Hsp90 for growth and/or survival of tumor cells. Hsp90 is a protein chaperone that helps a variety of client proteins to adopt their native conformation. Several co-chaperones such as Hop/Sti1, FKBP52, cyclophilin 40, and p50/Cdc37 are identified to be associated with Hsp90. These co-chaperones are required for binding to diverse client proteins and controlling the ATPase cycle of Hsp90 (4–6). Hsp90 is composed of three domains: an N-terminal domain of ~25-kDa, a middle domain of ~35-kDa, and a C-terminal domain of ~10-kDa (7). The ATP-binding site of Hsp90 is located in the N-terminal domain. Low molecular weight compounds that interfere with ATP-binding such as geldanamycin or radicicol inhibit the Hsp90 function by competing for the interaction site.

Many of the client proteins of Hsp90 are crucial elements of the cellular signal transduction pathway. Protein kinases represent the largest class of Hsp90 client proteins, and many have been shown to cause cancer when deregulated. These protein kinases depend on Hsp90 for their proper folding and functioning suggesting that Hsp90 itself is a valid anti-cancer target of pharmaceutical interest (8).

Hsp90 does not directly bind to protein kinases, but this interaction is mediated by the co-chaperone Cdc37/p50. Hence, Cdc37 has also been dubbed as a kinase targeting subunit of the Hsp90 machinery (9). Interestingly, Cdc37 is also able to act as a chaperone by itself independent of Hsp90 (10).

The cell division cycle protein 37 (Cdc37) was first identified in *Saccharomyces cerevisiae* as a protein required for the "Start" event in the cell division cycle (11). In yeast, *cdc37* mutations cause synthetic lethality (as defined by Kaelin (56)) in combination with thermosensitive *cdc28* or *kin28* mutations (12, 13). The mammalian homolog of Cdc37, also referred to as $p50^{cdc37}$, was first identified within a complex consisting of the Rous sarcoma virus encoded oncogene $pp60^{v\text{-}scr}$ and Hsp90 (14, 15). Further studies confirmed that protein kinases are the most favored targets of Cdc37 (16). A plethora of other oncogenic kinases, including Raf isoforms, Akt, and ErbB2, have been identified as potential clients of Cdc37 (17–20). Expression of Cdc37 is up-regulated in cancer cells and tissues and can promote tumorigenesis when overexpressed (21, 22). In addition, Cdc37 can inhibit the ATPase activity of Hsp90 implied in promoting the assembly of kinase clients with both chaperone proteins (23, 24).

Structurally, the 44.5-kDa protein Cdc37 can be dissected into three domains (10, 25). Proteolytic fingerprinting studies indicate that it is comprised of an N-terminal domain (residues 1–127 ($Cdc37_N$), 15.5 kDa), a middle domain (residues 147–276 ($Cdc37_M$), 16 kDa), and a C-terminal domain (residues 283–378 ($Cdc37_C$), 10.5 kDa). The middle domain $Cdc37_M$ is

* This work was supported by the SPINE (Structural Proteomics in Europe) project of the European commission and by the Cluster of Excellence: Macromolecular Complexes (Deutsche Forschungsgemeinschaft). The costs of publication of this article were defrayed in part by the payment of page charges. This article must therefore be hereby marked "*advertisement*" in accordance with 18 U.S.C. Section 1734 solely to indicate this fact.

The atomic coordinates and structure factors (codes 2W0G and 2K5B) have been deposited in the Protein Data Bank, Research Collaboratory for Structural Bioinformatics, Rutgers University, New Brunswick, NJ (http://www.rcsb.org/).

[1] Sanofi-Aventis Deutschland GmbH, Industriepark Höchst, Frankfurt am Main D-65926, Germany.

[2] To whom correspondence should be addressed: Tel.: 49-69-79829737; Fax: 49-69-79829515; E-mail: schwalbe@nmr.uni-frankfurt.de.

[3] The abbreviations used are: Hsp90, 90-kDa heat shock protein; Cdc37, cell division cycle protein 37; CSP, chemical shift perturbation; CST, cross-saturation transfer; HADDOCK, high ambiguity-driven biomolecular docking; HSQC, heteronuclear spin quantum correlation; NOE, nuclear Overhauser effect; NOESY, nuclear Overhauser effect spectroscopy; RDC, residual dipolar couplings; r.m.s.d., root mean square deviation; R_g^{theo}, radius of gyration (theoretical); R_g^{exp}, radius of gyration (experimental); SAXS, small angle x-ray scattering; TROSY, transverse relaxation-optimized spectroscopy; DTT, dithiothreitol; PAA, polyacrylamide.

highly resistant to proteolytic digestion and was found to be the most stable domain of Cdc37 (26). Several studies (19, 27–30) have shown that $Cdc37_N$ binds to the client proteins (*e.g.* kinases). A highly conserved region within $Cdc37_N$ contains Ser-13 as a unique phosphorylation site for the protein kinase CKII. Phosphorylation seems to be an important mechanism for controlling the binding affinity to the client protein kinases and as a consequence thereof regulating the activity of multiple protein kinases (31). The Hsp90 binding site is located in the middle domain of Cdc37, which also comprises a putative dimerization region (32). An extended α-helix connects the Hsp90 binding site to the C-terminal domain, which might also be required for dimer formation (24, 32). The structure of the N-terminal domain is yet unknown but sequence analysis predicts a high content of α-helices (32).

The crystal structure of $Cdc37_{MC}$ (middle and C-terminal domain) bound to $Hsp90_N$ (from yeast) is a heterotetrameric complex, comprising Hsp90 bound to a Cdc37 dimer (32). The function of Cdc37 to inhibit the ATPase activity of Hsp90 (24) is due to the extended side chain of Arg-167 that binds to Glu-33 of Hsp90, thereby inhibiting the ATPase reaction. Additional studies indicate that $Cdc37_M$ exists as a monomer (26). Low resolution cryoelectron microscopy images of the Hsp90·Cdc37·Cdk4 complex show that Cdc37 is a monomer in this interaction (33). However, these studies utilized yeast Hsp90, and it was realized that it is necessary to investigate the interaction with human Hsp90 (26) to resolve the differences.

Here, we report the structure determination of the human $Hsp90_N$·$Cdc37_M$ complex based on the NMR backbone assignments of $Cdc37_M$ (34) and $Hsp90_N$ (35). The interface of the complex between human $Cdc37_M$ and $Hsp90_N$ could be mapped based on NMR chemical shift perturbation (CSP) studies, and cross-saturation transfer (CST) techniques. Subsequently, we solved the x-ray crystal structure of human $Cdc37_M$ at 1.88 Å in its monomeric form. The structure of the $Cdc37_M$·$Hsp90_N$ complex was generated by incorporating NMR data (CSPs and CSTs as ambiguous distance restraints and RDCs as orientational restraints) in the HADDOCK (36) docking protocol.

EXPERIMENTAL PROCEDURES

Cdc37 Cloning, Expression, and Purification—From the cDNA (Invitrogen) the base pairs corresponding to amino acids 1–126, 147–276, 1–283, and 1–378 of human Cdc37 were amplified by PCR using 5′-ACACAACCATGGTGGACTACAGCGTGTGGGACCAC-3′, 5′-ACACAAGGATCCTTCACTTGCTGAAGCCGTCTTTGCTGAGC-3′, 5′-AAACCATGGGGAAACACAAGACCTTCGTGGAAAAATACG-3′, 5′-AAGCAAGGATCCTTCACTTCATGGCCTTCTCGATGCGCAG-3′, 5′-ACACAAGGATCCTTCAGCGCTCCTCCTCCTCGTACTCCTTC-3′, 5′-TCTTTATTTTCAGGGCGCCATGGTGGACTACAGCGT-3′, and 5′-GCAGCCGGATCCTTCACACACTGACATCC-3′ as primers, respectively. The PCR product was double digested with NcoI and BamHI and cloned into the derivatized pKM263 (6xHis tag ProtGB1-Tev between Nde1 and Xho1) vector, which harbors ProtGB1 to enhance the solubility of the expressed fusion partner. The authenticity of the clone construct was confirmed by nucleotide sequencing. *Escherichia coli* strain BL21(DE3) (Novagen) containing the desired plasmid was grown in Luria-Bertani (LB) broth medium at 37 °C supplemented with 34 μg/ml chloramphenicol. Protein expression was induced with the addition of 1 mM isopropyl 1-thio-β-D-galactopyranoside when the A_{600} reached 0.6–0.7. The culture was incubated in 5-liter Erlenmeyer flask for 5–6 h with aeration (160 rpm) at 37 °C before the cells were harvested by centrifugation (5,000 × *g*, 15 min, 4 °C). The cell pellet was resuspended in lysis buffer (50 mM Tris-HCl (pH 8.0), 0.5 M NaCl, 5 mM of β-mercaptoethanol) with addition of 2 mg/ml lysozyme and 100 units/ml benzonase (Merck, Darmstadt, Germany) protein suspension. After sonication (10×, 60-s pulse on, and 180-s pulse off) in an ice bath, the cell debris was removed by centrifugation (18,000 × *g*, 45 min, 4 °C) to yield a supernatant containing the soluble protein. The supernatant was applied to a nickel-nitrilotriacetic acid FastFlow column (Qiagen) following the manufacturer's recommendations. After Tev-protease cleavage to remove the His tag ProtGB1, the protein was applied again on a nickel-nitrilotriacetic acid column. The pooled protein fractions were further purified by gel filtration on a Hiload 26/60 Superdex 75 preparative grade column (Amersham Pharmacia Biosciences) in Hepes 50 mM (pH 7.5), NaCl 100 mM, and 1 mM DTT. The protein-containing fractions were pooled, concentrated, and either immediately used for the experiments or stored at −20 °C. The ^{15}N-labeled protein was produced by using M9 minimal media with $^{15}NH_4Cl$ (1 g/liter) as the sole nitrogen source. Uniformly triple (^{2}H,^{13}C, and ^{15}N) or double (^{2}H and ^{15}N) labeled protein was produced using Silantes OD2 media. The degree of isotopic enrichment for the Silantes media was >98% for all isotopes (manufacturer's data). For selective labeling with ^{15}N-labeled amino acids, the following ^{15}N-labeled amino acids were used: alanine, arginine, lysine, methionine, isoleucine, leucine, valine, phenylalanine, tyrosine, and tryptophan (Spectra Stable Isotopes, Germany). The procedure applied for selective amino acid labeling is essentially the same as described in the literature (37).

$Hsp90_N$ Cloning, Expression, and Purification—From the cDNA (Stratagene) the base pairs corresponding to amino acids 18–223 (N-terminal domain) of human Hsp90 were amplified by PCR using 5′-AAACCATGGGGGAGACGTTCGCCTTTCAGG-3′ and 5′-GCAGCCGGATCCTCACTCCACAAAAAGAG-3′ as primers. The PCR product was double digested with NcoI and BamHI and was cloned into the derivatized pKM263, with a Protein G B1 domain (ProtGB1) fusion protein located C-terminally behind a stretch of six histidines and a tev cleavage site under the control of a T7-promoter (see above). The protein was expressed and purified in the same way as Cdc37, except for the post induction temperature, which was 25 °C. In addition, tetra-selective labeling with ^{15}N-glycine, ^{15}N-alanine, ^{15}N-phenylalanine, and ^{15}N-leucine was carried out as described above.

Due to the design of the expression vectors, Cdc37 and $Hsp90_N$ constructs carry two (GA) or four (GAMG) additional amino acids at the N terminus. High expression levels were achieved after induction with 1 mM isopropyl 1-thio-β-D-galactopyranoside at 37 °C for Cdc37 and 25 °C for $Hsp90_N$ and ~95% of the fused protein was found in the soluble fraction.

Typically, 30 mg/liter of pure (95%) proteins was obtained after cleavage of protein G. The final samples were dialyzed against the NMR buffer (Hepes 50 mM (pH 7.5), NaCl 100 mM, and 1 mM DTT).

Mutagenesis—Mutants of $Cdc37_M$ were created with QuikChange kit (Stratagene), and sequenced to confirm the incorporation of the correct mutation. The mutant proteins were purified following the same protocol as the wild-type $Cdc37_M$.

NMR Spectroscopy—NMR experiments were performed at 298 K, on Bruker 600-, 700-, 800-, 900-, and 950-MHz spectrometers equipped with cryogenic triple-resonance probes. For the $Cdc37_M$·$Hsp90_N$ complex a ratio of 1:1 was used for all measurements. The spectrometer was locked on D_2O. The spectra were processed using Topspin 2.0 (Bruker Biospin) and analyzed using either SPARKY 3.113[4] or CARA 1.8.3 (39). The resonances for the free form of $Cdc37_M$ at pH 5.5 and $Hsp90_N$ at pH 7.5 have been assigned before (34). Spectra of $Cdc37_M$ at pH 7.4 have been assigned by performing a pH series (5.0, 5.5, 6.0, 6.5, 7.0, 7.5, and 8.0) with 2,2-dimethyl-2-silapentane-5-sulfonic acid as an internal standard for calibration. Sequential backbone assignment of ^{15}N-labeled $Cdc37_M$ in complex with unlabeled $Hsp90_N$ and *vice versa* was achieved by overlaying the $^1H,^{15}N$-HSQC spectra of free $Cdc37_M$ (or $Hsp90_N$) and $Cdc37_M$ (or Hsp90) in complex and verified by the NOE patterns from a high resolution three-dimensional $^1H,^{15}N$-NOESY HSQC spectrum and selective ^{15}N-amino acid labeling (alanine, arginine, glycine, isoleucine, leucine, lysine, methionine, phenylalanine, tryptophan, tyrosine, and valine). Additionally, a three-dimensional $^1H,^{15}N$-NOESY HSQC spectrum for $Hsp90_N$ with a tetra-selectively labeled sample in which only glycine, alanine, phenylalanine, and leucine were ^{15}N-labeled was used to assist the assignment. $^1D(H,N)$ RDCs were measured for the $Cdc37_M$·$Hsp90_N$ complex (in which both proteins were ^{15}N-labeled) in pf1 phage (5 g/liter, Profos) and in 4% polyacrylamide (PAA) gel alignment media at 700 MHz. The $^1D(H,N)$ were extracted from IPAP-($^1H,^{15}N$)-HSQC spectra (40, 41). Signals that could be traced back reliably and determined unambiguously were analyzed using MODULE (42) and PALES (43). CST experiments were carried out at 25 °C according to the procedure of Takahashi *et al.* (57). The sample contained 1 mM of $^2H,^{15}N,^{13}C$-labeled $Cdc37_M$ protein with the unlabeled $Hsp90_N$ protein in $^1H_2O/^2H_2O$ (1:9, v/v) containing 50 mM Hepes (pH 7.5), 1 mM DTT, and 100 mM NaCl. The Gaussian pulse scheme was used for saturation of aliphatic protons with irradiation frequency set to 1.1 ppm. A saturation time of 2.0 s was employed.

X-ray Crystallography—Initial screening for crystallization conditions of $Cdc37_M$ was performed using screening kits purchased from JB (Jena Bioscience). These trials were successful, with five promising conditions producing crystals. The protein samples that did not give crystals were analyzed by mass spectrometry, which identified that they contained small fractions of proteins with an increased molecular mass of ~75, 150, and 228 Da. We attributed this observation to the formation of mixed disulfides of β-mercaptoethanol with the four free cysteines of $Cdc37_M$. Therefore, β-mercaptoethanol was omitted from the further protein preparations. The final diffracting quality crystals were grown from $Cdc37_M$ (Hepes, 50 mM, NaCl, 100 mM, pH 7.5, "protein buffer") at a final concentration of 1.1 mM, in solution containing Hepes, 100 mM, pH 7.5, sodium acetate, 100 mM, 22% polyethylene glycol 4000, ("reservoir buffer"). Crystal drops were setup using the sitting drop vapor diffusion method at 18 °C. Crystals were transferred in a stepwise manner into solutions of increasing glycerol concentrations of 5, 10, 15, 20, and 25%, respectively, based on one volume of protein buffer and two volumes of reservoir buffer, and flash-cooled in an X-Stream 2000 nitrogen stream at 140 K. Diffraction data were collected using a Rigaku R-Axis IV image plate detector at a wavelength of 1.5418 Å (CuKα radiation from a MicroMax-007 Microfocus generator). In addition to a high exposure data set consisting of 360 images of 1.0° rotations, a low exposure (one-third of the exposure time per image of that for high exposure) data set was collected consisting of 240 images of 1.5° rotations. The oscillation images were processed with the HKL/DENZO program package (44). The crystals belong to the hexagonal space group $P6_1$ with unit cell dimensions a = b = 48.67 Å and c = 104.26 Å. Scaling and merging of the oscillation images was performed with SCALEPACK (44). Data reduction and approximate absolute scaling of the data were performed with TRUNCATE from the CCP4 program suite (45). The phase problem was solved by molecular replacement using the program AMoRe (46) from the CCP4 suite, the diffraction data between 15 Å and 3 Å resolution, and a Cdc37 search model constructed from PDB entry 1US7 (32), extending from residue His-148 to residue Lys-276 and consisting of 1086 non-hydrogen atoms. The top solution with rotation angles $\alpha = 45.52°$, $\beta = 150.55°$, $\gamma = 311.52°$ and translations $T_x = -0.3117$ and $T_y = 0.0954$ (fractional coordinates) was associated with a correlation coefficient of 58.2% and an *R*-factor of 40.4%. After rigid body refinement with Refmac5 (47), the *R*-factor for the data between 42.14 Å and 1.88 Å was 43.8% ($R_{free}T = 43.9\%$). After several cycles of restrained refinement with Refmac5, the modeling of tightly bound water molecules, and manual rebuilding with COOT (48), the final structure was obtained.

Docking—Calculation of the $Cdc37_M$·$Hsp90_N$ complex was achieved using a high ambiguity driven docking (HADDOCK 2.0) approach with CNS 1.1 (49) essentially as described in the literature (36). The ambiguous interaction restraints have been defined for the residues that exhibited significant NMR amide chemical shift changes and/or strong saturation transfer upon interaction with its partner protein. For Hsp90, residues 117, 121, 123, 124, 125, 126, and 129 have been defined as active and residues 28, 32, 40, 46, 51, 54, 55, 114, 116, 119, 120, 122, 127, 130, 132, 133, and 134 as passive. The helix (112–124) and adjacent loop region from residues 106–127 were left fully flexible to offer freedom to the orientation of this helix. Additional hydrogen-bond restraints were added to keep the secondary structure of this helix. For $Cdc37_M$, residues 160, 161, 164, 165, 166, 167, 168, 193, 202, 204, 205, and 208 have been defined as active and residues 156, 157, 158, 169, 170, 174, 189, 192, 196, 197, 200, 201, 203, 207, 211, 242, and 249 as passive. The loop region 164–168 was left fully flexible during the docking. One

[4] T. D. Goddard and D. G. Kneller, SPARKY 3, University of California, San Francisco.

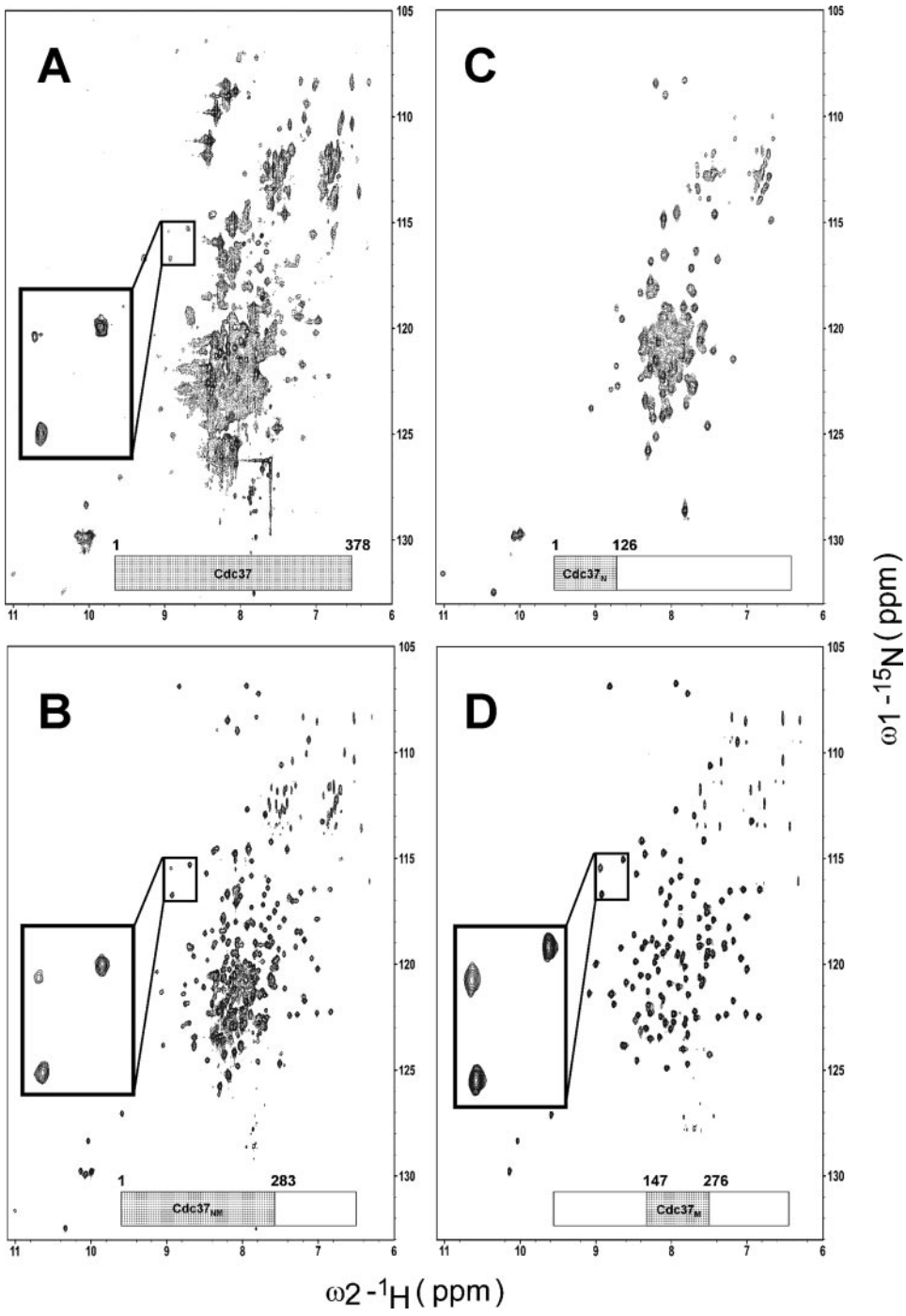

FIGURE 1. **$^{1}H,^{15}N$-TROSY spectra (950 MHz) of different Cdc37 constructs.** The boundaries of each construct (*e.g. A*, full-length; *B*, N-terminal and middle domain; *C*, N-terminal domain; and *D*, middle domain) are schematically indicated below each spectrum. The *insert* shows three peaks stemming from the middle domain ($Cdc37_M$) showing the same fold for this domain in all constructs. The spectra were acquired at 298 K in the same buffer solution (50 mM Hepes buffer (pH 7.5), 100 mM NaCl, 1 mM DTT, and 10% D_2O).

intermolecular NOE (Ala-117-HN to Ala-204-HB), as obtained from NOESY experiments, fitted very well with the initial docking results and was included in the final calculation. To enhance the convergence, $^{1}D(H,N)$ RDCs obtained both in 4% PAA gel and in 5 g/liter pf1 phage alignment media, were included in the calculation and the axial (D_a) and rhombic (D_r) components of the alignment tensor were estimated using PALES (43). For the initial rigid-body docking, only the RDCs in the stable secondary structure elements were used, whereas in the further refinement steps, all RDCs were used. The final values for D_a and D_r were −8.21 and 0.62 for the phage alignment and 9.39 and 0.45 for the alignment in the PAA gel. The dockings were performed using our $Cdc37_M$ crystal structure and the Hsp90 crystal structure (pdb: 1YES) (7). The protein allhdg 5.3 force field (50) was used for the calculations. The 200 final water-refined docking results are clustered at the interface within a threshold of 3.0 Å pairwise backbone r.m.s.d. The top-ranked ensemble, according to the average interaction energy and buried surface area, was accepted as the best representative of the complex.

RESULTS

Comparing Different Constructs of Cdc37 and Hsp90—The study of the rather large complex formed between the 45-kDa Cdc37 protein and the 23-kDa N-terminal domain of Hsp90 is a challenge for NMR spectroscopic studies. To study this complex, we reduced the boundaries of Cdc37 to obtain a construct that retains its structural and functional properties and is suitable for NMR studies. Beside the $Hsp90_N$ binding domain of Cdc37 (147–276, $Cdc37_M$), for which we recently published the NMR assignments (34), also the following Cdc37 constructs were investigated: full-length Cdc37 (1–378), the kinase binding domain (1–126, $Cdc37_N$), and both kinase and $Hsp90_N$ binding domains (1–283, $Cdc37_{NM}$). The suitability of the Cdc37 constructs for NMR was investigated by recording $^{1}H,^{15}N$-TROSY spectra (Fig. 1). The spectrum of the full-length Cdc37 revealed considerable signal overlap and, in addition, signals that indicate unfolded regions (Fig. 1*A*). For $Cdc37_N$, the spectrum shows again signal overlap and evidence for a high content of partially unfolded and/or helical regions (Fig. 1*C*). $Cdc37_M$ shows a nicely resolved high resolution $^{1}H,^{15}N$-TROSY spectrum (with 131 out of the 133 expected amide resonances), which indicates that this Hsp90-binding domain of Cdc37 is properly folded (34) (Fig. 1*D*). It was suspected that the $Cdc37_N$ might become more structured when it is together with the middle domain. Nevertheless, for

TABLE 1
Crystallographic data collection and refinement statistics

	All data	Highest resolution bin
Data		
Resolution limits (Å)	42.14-1.88	1.95-1.88
No. of measured reflections	368,290	41,732
No. of unique reflections	11,278	1,134
Redundancy	32.7	36.8
Completeness (%)	98.7	100
Completeness with I $>2\sigma$ (%)	94.1	86.1
I/σ(I)	49.8	18.7
R_{sym} (%)	5.8	30.6
B value from Wilson plot (Å^2)	35.5	
Mosaicity (°)	1.1	
Solvent content (%)	43	
Refinement		
Resolution limits (Å)	42.14-1.88	1.93-1.88
Test set selection	Random (5% = 609)	Random (5% = 46)
R_{free}T (%)	24.6	45.0
R_{work} (%)	21.2	29.1
$R_{work+test}$ (%)	21.3	
Number of non-hydrogen atoms	1130	
Mean B value (Å^2)	29.3	
r.m.s.d. values		
From ideal bond lengths (Å)	0.018	
From ideal bond angles (°)	1.544	
Ramachandran plot		
Favorable (%)	93.2	
Additional (%)	6.8	
Generous (number)	0	
Disallowed (number)	0	

the corresponding $Cdc37_{NM}$ construct the $^1H,^{15}N$-TROSY spectra indicated insufficient chemical shift dispersion (Fig. 1*B*). The amide signals originating from $Cdc37_M$ (shown specifically for three peaks as in the *insert* in Fig. 1*D*) have the same chemical shifts as in the full-length Cdc37 and $Cdc37_{NM}$ (Fig. 1, *A* and *B*), indicating that the fold of the $Cdc37_M$ is the same as in the full-length protein. Hence, the 16-kDa $Cdc37_M$ domain was used for all further NMR experiments. For Hsp90, the 23-kDa construct comprising the N-terminal ATP-binding domain (18–223) known to interact with Cdc37 was used throughout this study (35).

Structure of Human $Cdc37_M$—In the x-ray structure of the complex between yeast Hsp90 and human Cdc37, the middle domain of the Cdc37 protein forms a homodimeric interaction with a symmetry-related molecule (32). So far, the structure of Cdc37 is only available in the complex with Hsp90. However, by NMR, we do not see any evidence for dimer formation of $Cdc37_M$. To elucidate whether $Cdc37_M$ also forms dimers when crystallized without Hsp90, we solved the x-ray structure of free $Cdc37_M$. The obtained resolution after refinement was 1.88 Å with the characteristics summarized in Table 1. The structure of $Cdc37_M$ is entirely helical consisting of a 6-helix bundle (148–243) connected to a single long helix (245–276) as shown in Fig. 2. In the crystals, $Cdc37_M$ is a monomer, which is in excellent agreement with NMR diffusion-based measurements showing that $Cdc37_M$ exists as a monomer in solution with an $R_g^{exp} = 21.3$ Å and a theoretical (51) predicted $R_g^{theo} = 22.2$ Å. These findings agree very well with previous findings based on SAXS (26) and electron microscopy (33) data. The overall structure of this free-form monomeric $Cdc37_M$ is very similar to the x-ray structure of the dimeric $Cdc37_M$ when in complex with the yeast Hsp90 (32). The average r.m.s.d. between the structures for all heavy atoms is 0.8 Å for the 6-helix bundle (148–243) and 1.3 Å for the full domain (148–276). The largest differences are observed in the loop connection (242–251) to the single long α_7 helix, which is exactly at the previously proposed dimerization interface (32). Interestingly, this region is also near to Hsp90 and may thus expose a potential additional interaction site. Furthermore, we found two possible conformations for the side chains of Arg-167 and Gln-208 in the $Cdc37_M$ crystals, which are also slightly different from the conformation found in the previously reported structure. Both residues reside in and near the interaction interface with Hsp90.

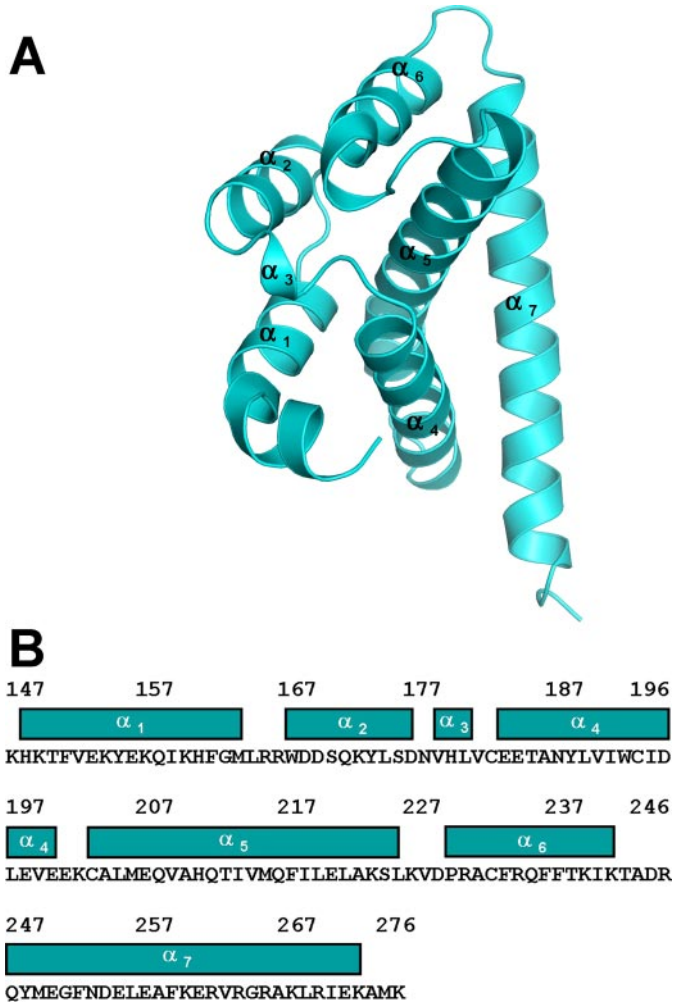

FIGURE 2. **X-ray structure of $Cdc37_M$.** *A*, x-ray structure of $Cdc37_M$ in *ribbon representation*. The helices are indicated. *B*, the amino acid sequence and the secondary structure boundaries of $Cdc37_M$ are represented schematically.

Assignment of Human $Cdc37_M$ and Human $Hsp90_N$—The $^1H,^{15}N$ and ^{13}C backbone and side-chain resonance assignment of the free-form $Cdc37_M$ has been reported previously at pH 5.5 (34). Because the interaction studies with $Hsp90_N$ have to be conducted at pH 7.5, we reassigned the amide resonances of $Cdc37_M$ at this different condition. Hence, we performed a series of NMR experiments ranging from pH 5.0 through pH 8.0 with a 0.5 pH unit increment, and used 2,2-dimethyl-2-silapentane-5-sulfonic acid as an internal standard for calibration. Using the $^1H,^{15}N$-HSQC spectra from the pH series we

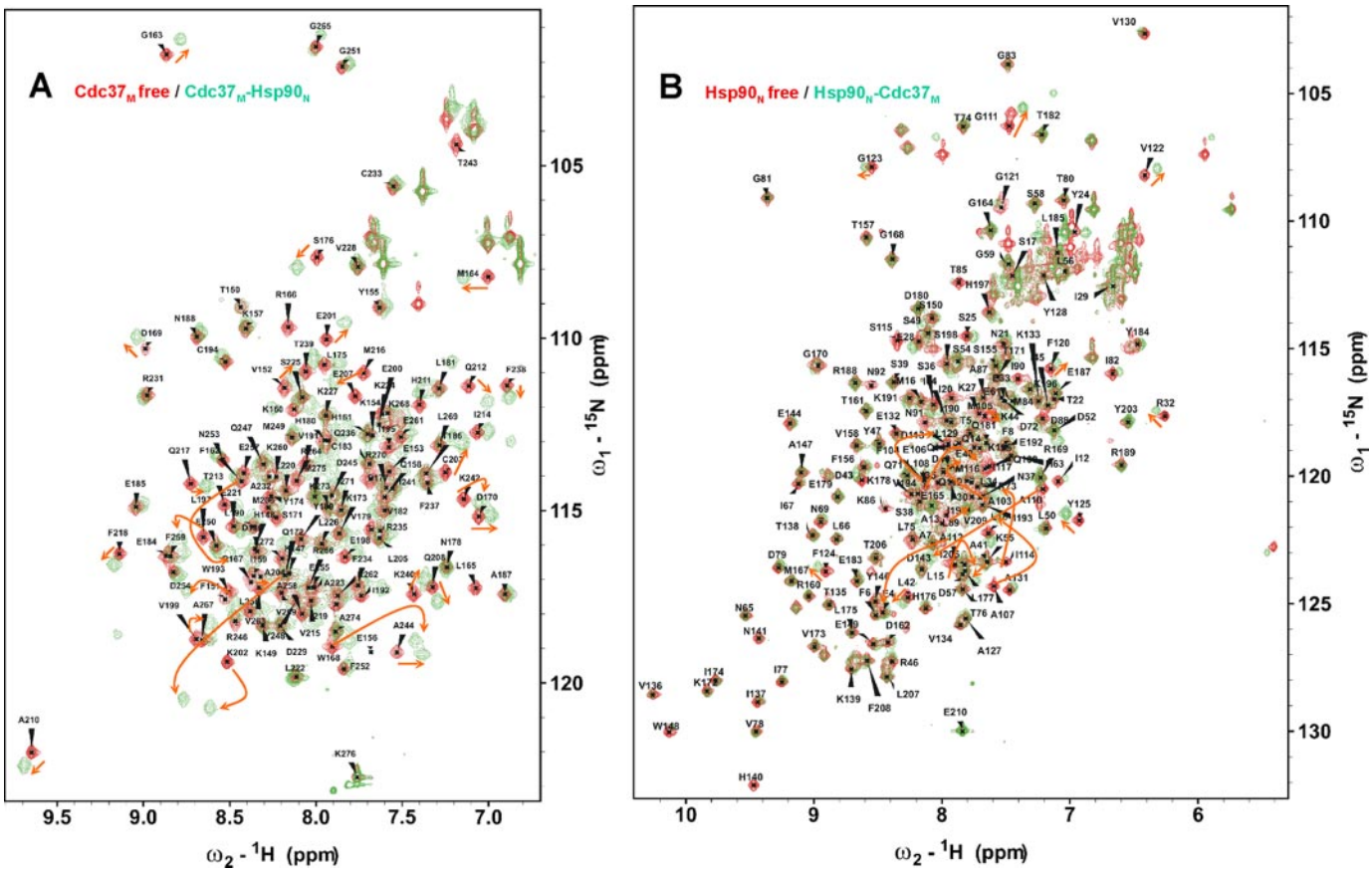

FIGURE 3. **Cdc37$_M$ binding to Hsp90$_N$.** Overlay of the ^{1}H,^{15}N-HSQC spectra (900 MHz)of Cdc37$_M$ in its free form(*red*) with Hsp90$_N$ bound form(*green*) (*A*) and of Hsp90$_N$ in its free (*red*) with Cdc37$_M$-bound form (*green*) (*B*). The backbone assignments are shown for the free form of Cdc37$_M$ (*A*) and Hsp90$_N$ (*B*), and some of the major peak shifts are indicated by *arrows*. The spectra were acquired at 298 K in the same buffer solution (50 mM Hepes buffer (pH 7.5), 100 mM NaCl, 1 mM DTT, and 10% D_2O).

were able to nearly completely assign Cdc37$_M$ (99% of the backbone amide resonances) at pH 7.5.

The ^{1}H,^{15}N and ^{13}C backbone and side-chain resonances of the human Hsp90$_N$ (18–223) at pH 7.5 in its free form have been assigned previously (35). The amide backbone assignment was complete with the exception of four stretches (Gln-23 to Glu-25, Leu-107 to Lys-116, Ser-165 to Gly-168, and Phe-213 to Tyr-216) and the amino acids Phe-37, Asn-40, Leu-45, Thr-65, Lys-74, Leu-76, Lys-84, Gly-132, Phe-138, Ser-140, Asp-156, Thr-176, Glu-199, and Gln-212.

Mapping of the Binding Interface of the Cdc37$_M$/Hsp90$_N$ Complex by NMR—To map the Cdc37$_M$ binding site for Hsp90$_N$, NMR titrations were performed with ^{15}N-labeled Cdc37$_M$ and unlabeled Hsp90$_N$ at 25 °C and pH 7.5. An overlay of the ^{1}H,^{15}N-HSQC spectra of free Cdc37$_M$ and the Cdc37$_M$·Hsp90$_N$ complex is shown in Fig. 3*A*. These spectra reveal significant changes in the combined amide chemical shifts (^{1}H,^{15}N) of the Cdc37$_M$ upon addition of Hsp90$_N$ (up to a molar ratio of 1:1). Many peaks in the two-dimensional ^{1}H,^{15}N-HSQC spectrum of Cdc37$_M$ are either significantly shifted or disappear (exchanged broadened) from the spectra indicating complex formation. The assignment of the shifted peaks was confirmed by using a combination of ^{15}N amino acid-selective labeling and three-dimensional ^{1}H,^{15}N-NOESY-HSQC spectra. To facilitate the assignment in the complex, Cdc37$_M$ was selectively labeled with ten different ^{15}N-labeled amino acids (Ala, Arg, Ile, Leu, Lys, Met, Phe, Trp, Tyr, and Val). Except for those signals that broadened beyond detection, all other peaks could be assigned unambiguously. The residues of Cdc37$_M$ revealing the largest combined (^{1}H,^{15}N) chemical shift perturbation (CSP $>$ 0.15 ppm) upon binding Hsp90$_N$ are Phe-162, Arg-167, Trp-168, Trp-193, Lys-202, Ala-204, Val-209, and Met-216 (Fig. 4*A*). Furthermore, amino acids Leu-165, Arg-166, Ile-195, Leu-205, and Glu-207 show a strong decrease in signal intensity. To further analyze the interaction site of Cdc37$_M$, we performed a CST experiment. This experiment was carried out using ^{2}H,^{15}N,^{13}C-labeled Cdc37$_M$ protein with the unlabeled Hsp90$_N$ protein in $^1H_2O/^2H_2O$ (1:9, v/v). The Cdc37$_M$ residues that appear to be in the interface ($<$0.78 intensity ratio) region include Lys-160, Met-164, Arg-166, Arg-167, Trp-168, Leu-205, Glu-207, Gln-208, and Ile-214 (Fig. 4*B*). When we combine CSPs, CSTs, and the decrease of signal intensity and map the binding site onto the Cdc37$_M$ crystal structure, two distinct regions appear to be involved in complex formation. The first region is composed of the loop (residues 164–167), and the second region is defined by the loop connecting α-helices 3 and 4 and the beginning region of the α-helix 4 (residues 203–208).

The reciprocal experiments using ^{15}N-labeled Hsp90$_N$ and unlabeled Cdc37$_M$ to identify the residues of human Hsp90$_N$ involved in the interaction with the Cdc37$_M$ were carried out as well. An overlay of the ^{1}H,^{15}N-HSQC spectra of free Hsp90$_N$

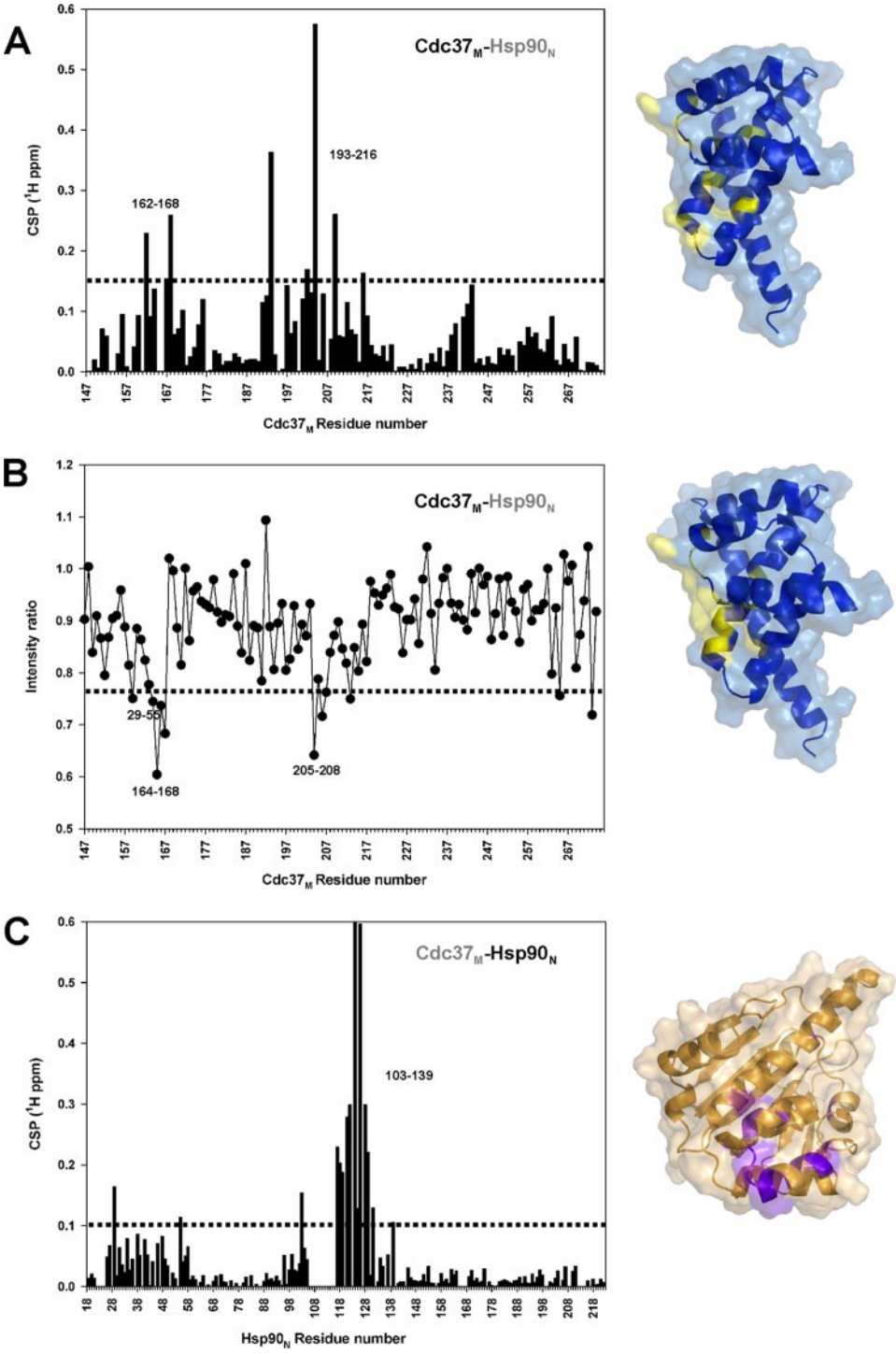

FIGURE 4. **Titration of $Cdc37_M$ with $Hsp90_N$ and *vice versa*.** *A*, correlation of CSPs *versus* residues in $Cdc37_M$ upon addition of $Hsp90_N$ (*left*) and surface representation of the interaction sites of $Cdc37_M$ (*yellow*) for $Hsp90_N$ (>0.15 ppm). *B*, plot of the intensity ratios of the cross-peaks in the cross-saturation transfer experiment (*left*). The intensity ratios of the backbone amide resonance of $Cdc37_M$ in complex with $Hsp90_N$ with irradiation to those of without irradiation measured in 10% H_2O/90% D_2O. Surface representation of $Cdc37_M$, where residues with intensity ratio of <0.78 are colored in *yellow* (*right*). *C*, correlation of CSPs *versus* residues in $Hsp90_N$ upon addition of $Cdc37_M$ (*left*) and surface representation of the interaction sites of $Hsp90_N$ (*purple*) for $Cdc37_M$ (>0.1 ppm). For the CSPs, amide ^1H and ^{15}N resonance shifts have been mapped and combined as Euclidian distances between peak maxima taking into account the gyromagnetic ratio of proton and nitrogen (in ^1H ppm). *Missing bars* indicate prolines or amide resonances that have not been assigned.

and the $Hsp90_N$·$Cdc37_M$ (molar ratio 1:1) complex is shown in Fig. 3*B*. The shifted amide resonances of $Hsp90_N$ were assigned using a combination of selectively labeled samples and three-dimensional ^1H,^{15}N-NOESY-HSQC spectrum. $Hsp90_N$ was selectively labeled with six different ^{15}N-labeled amino acids (Ala, Gly, Ile, Leu, Met, and Phe). An additional three-dimensional ^1H,^{15}N-NOESY-HSQC spectrum was recorded for a sample in which four different amino acids (Ala, Gly, Phe, and Leu) were selectively ^{15}N-labeled. The $Hsp90_N$ amide CSPs upon binding to $Cdc37_M$ were analyzed to characterize the amino acids potentially involved in the interaction. The largest combined (^1H,^{15}N) chemical shift changes (>0.10 ppm) are observed for a few residues in the first, second, and fifth α-helix (residues 29, 55, and 103, respectively), and many residues in the sixth α-helix (residues 117–119 and 121–126) as well as in the seventh α-helix (residues 128, 129, and 131). These residues define two distinct $Hsp90_N$ interacting sites for $Cdc37_M$, which are located on one side of the molecule and are localized around a hydrophobic patch (Fig. 4*C*).

Determination of the Human $Cdc37_M$·$Hsp90_N$ Complex Structure—Based on the interaction interface as determined from CSPs and CSTs (Fig. 5, *A* and *B*) we calculated the structure of the binary $Cdc37_M$·$Hsp90_N$ complex using HADDOCK (36). The calculations were performed using the crystal structures of human $Cdc37_M$ determined here and $Hsp90_N$ in the open conformation (pdb: 1YES (7)). The initial docking model proposed a number of possible solutions that differed in the relative orientation of the proteins (Fig. 5*C*). To resolve this ambiguity, we measured two sets of RDCs of the complex. RDCs could be obtained using either 5 g/liter phage pf1 phage alignment medium (Profos) or alignment in 4% polyacrylamide gels. Both sets of ^1D(N,H) RDC values were extracted from IPAP-(^1H,^{15}N)-HSQC spectra and yielded a linearly independent overall alignment tensor (Fig. 5*C*) and thus provided additional information on the relative orientation of the two proteins. The RDCs have been measured on a sample containing both ^{15}N-labeled $Cdc37_M$ and ^{15}N-labeled $Hsp90_N$ in a 1:1 ratio.

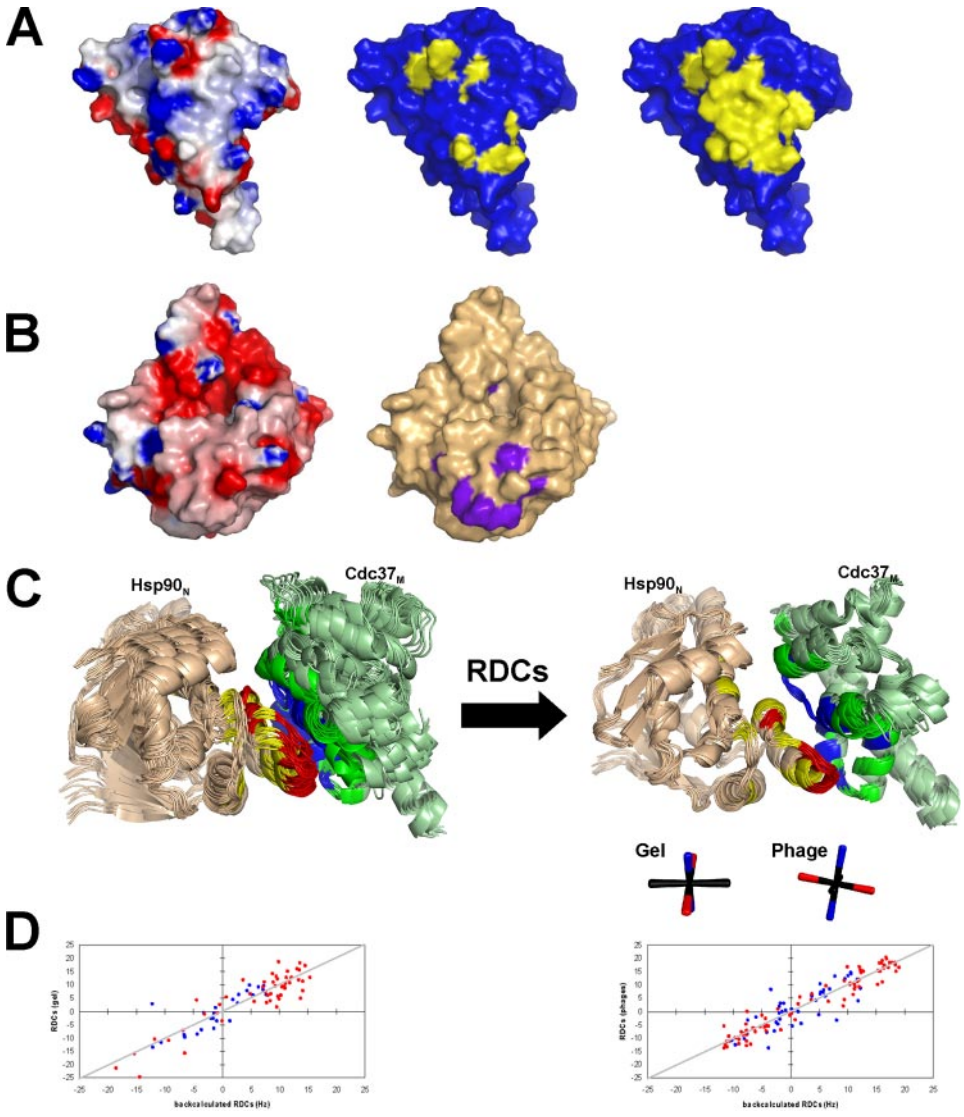

FIGURE 5. **NMR data driven docking model of human $Cdc37_M$·$Hsp90_N$ complex.** *A*, surface representation of $Cdc37_M$. *Left*: The molecular surface is *color-coded* by electrostatic potential, as calculated with DELPHI (38). Potentials less than −10 kT are *red*, those greater than +10 kT are *blue*, and neutral potentials (0 kT) are *white*. The *color* in between is produced by linear extrapolation. *Middle*, CSPs from Fig. 4*A* (>0.15 ppm) in *yellow* mapped onto the structure. *Right*, cross-saturation transfer experiment (Fig. 4*B*) in which residues with intensity ratios <0.78 are mapped onto the surface (*yellow*). *B*, surface representation of human $Hsp90_N$ (1YES.pdb). *Left*, the molecular surface is *color-coded* by electrostatic potential, as calculated with DELPHI (38). *Right*, CSPs from Fig. 4*C* (>0.1 ppm) in *purple* mapped onto the structure. *C*, bundle of the $Cdc37_M$·$Hsp90_N$ complex as obtained using HADDOCK, with and without using RDCs. For the calculation without RDCs (*left*), the ten best docking results for each of the two major HADDOCK clusters are shown, and for the calculation with RDCs (*right*) the ten best docking results are shown. The active/passive restraints were used as defined under "Experimental Procedures" and are *colored*, respectively, in *red* and *yellow* for $Hsp90_N$ or *blue* and *dark-green* for $Cdc37_M$. The RDC tensors for alignment in either polyacrylamide (PAA) gel or pf1 Phages are indicated below. *D*, correlation of the experimental *versus* back calculated RDCs for the free-form x-ray structures of $Cdc37_M$ (*blue*) and $Hsp90_N$ (*red*). Protons were added to the x-ray structures using CNS 1.1 (49) without using the RDCs. RDCs were back-calculated using the program PALES (43) with the bestFit option. *Left*: correlation plot in PAA gel alignment medium with Cdc37 in *blue* (25 RDCs, correlation coefficient of 0.822) and $Hsp90_N$ in *red* (52 RDCs, correlation coefficient of 0.903). *Right*: correlation plot in pf1 phages alignment medium with Cdc37 in *blue* (42 RDCs, correlation coefficient of 0.816) and $Hsp90_N$ in *red* (79 RDCs, correlation coefficient of 0.964).

already very well with the free-form protein structures of $Cdc37_M$ and $Hsp90_N$ (Fig. 5*D*) indicating that their overall structure will not change much when in complex. In addition to the RDCs, we measured intermolecular NOEs. Two-dimensional ^{15}N-edited NOESY spectra were recorded for the free $^{15}N,^{2}H$ $Cdc37_M$ and $Hsp90_N$ proteins as well as two-dimensional and three-dimensional ^{15}N-filtered NOESY spectra for the $^{15}N,^{2}H$-labeled protein when in complex with the $^{14}N,^{1}H$ (unlabeled) partner. In these experiments, we could identify several intermolecular cross-peaks. However, because no full side-chain assignment is available, in most cases we could not unambiguously assign them. Based on dockings using the interaction interface either with or without the RDCs, we included one strong intermolecular NOE as observed for $Hsp90_N$ Ala-117-HN to $Cdc37_M$ Ala-204-HB in the final docking calculation.

In the final docking calculations, the active and passive residues in the interaction site and the flexible interfaces have been included as stated in under "Experimental Procedures" as well as both sets of RDCs and the strong intermolecular NOE. The top-ranked docking model for the $Cdc37_M$·$Hsp90_N$ complex (Fig. 5*C*) shows the preferential binding mode and includes 185 out of 200 final structures when clustered within the 3.0 Å pairwise backbone r.m.s.d. These final structures have been analyzed whether they satisfy the biochemical and structural restraints. The active residue 168 of $Cdc37_M$ causes violations at a 2 Å ambiguous interaction restraint cut-off, but is still acceptable at a distance of 3 Å from $Hsp90_N$.

$Cdc37_M$-$Hsp90_N$ Interface and Structural Reorganization upon Complex Formation—The interface between $Cdc37_M$ and $Hsp90_N$ buries a total surface area of 1579 ± 92 Å^2, which is highly comparable to the interface for the average protein·protein complex (1600 ± 400 Å^2) (52). There are two main $Cdc37_M$·$Hsp90_N$ interaction regions that together form the interface. The hydrophobic core is mainly formed by the interaction of $Cdc37_M$ residues in the α_4 and α_5 helix with the residues in the $Hsp90_N$ α_6 helix and adjacent

Although some amide signals of both proteins overlap, there is sufficient dispersion to identify many residues from $Cdc37_M$ or $Hsp90_N$. In the phage alignment media, we could reliably identify 42 $^{1}D(N,H)$ RDCs for $Cdc37_M$ and 79 $^{1}D(N,H)$ RDCs for $Hsp90_N$. Despite the line broadening in the polyacrylamide gel alignment, we could reliably identify 25 $^{1}D(N,H)$ RDCs for $Cdc37_M$ and 52 $^{1}D(N,H)$ RDCs for $Hsp90_N$. The RDCs fit

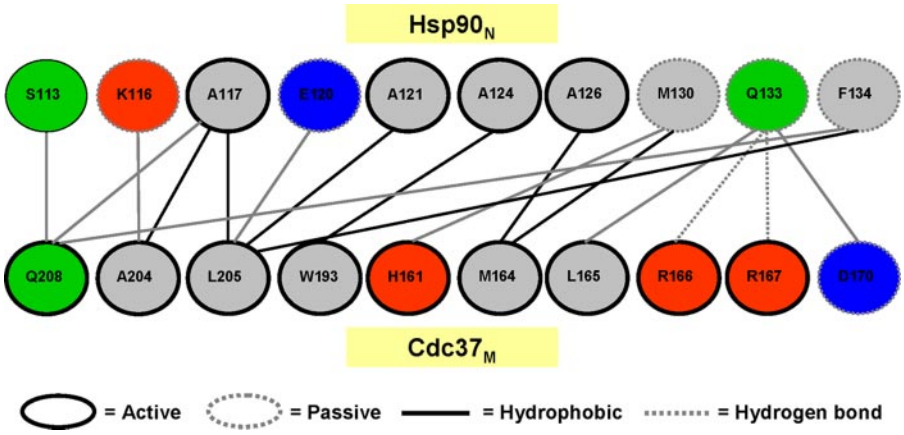

FIGURE 6. **Schematic representation of the interaction interface of NMR calculated $Cdc37_M$·$Hsp90_N$ complex structure.** The positively charged, negatively charged, neutral, and hydrophobic amino acids are colored in *red*, *blue*, *green*, and *gray*, respectively.

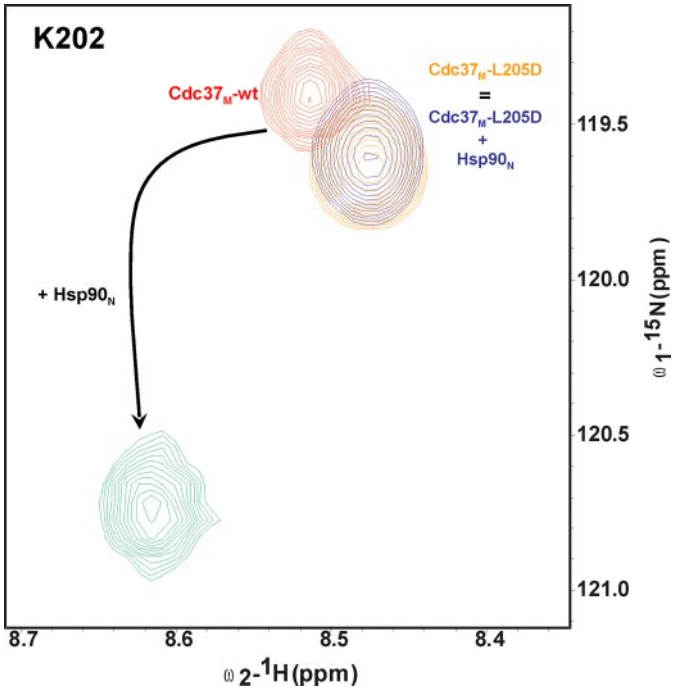

FIGURE 7. **$Cdc37_M$-L205D mutant does not bind to $Hsp90_N$.** ^1H,^{15}N-HSQC spectral region showing the amide signal for Lys-202, for wild type-free (*red*), mutant-free (*orange*), wild type in complex with $Hsp90_N$ (1:1) (*green*), and mutant in the presence of $Hsp90_N$ (1:4) (*blue*).

residues. Additionally, the $Cdc37_M$ α_1, α_2 helices and connecting loop interact with the $Hsp90_N$ α_7 helix and adjacent loop regions, involving many charged residues. Our docking results show an ensemble with many electrostatic and hydrophobic contacts as shown in Fig. 6. Electrostatic interactions are generally observed between the residues Arg-166, Arg-167, and Asp-170 of $Cdc37_M$ and Gln-133 of $Hsp90_N$ (hydrogen bonds are often observed for $Cdc37_M$ residues Arg-166 and Arg-167 to residue Gln-133 of $Hsp90_N$). The hydrophobic core involves residues Met-164, Trp-193, Ala-204, and Leu-205 of $Cdc37_M$ and Ala-117, Ala-121, Ala-124, Ala-126, Met-130, and Phe-134 of $Hsp90_N$. Upon $Hsp90_N$ binding, there are no large conformational changes in $Cdc37_M$, except in the flexible loop regions of the molecule. When superimposing the $Cdc37_M$·$Hsp90_N$ complex onto the uncomplexed molecules (coordinates from our $Cdc37_M$ crystal structure and 1YES for $Hsp90_N$), the r.m.s.d. on the C_α atoms is 0.7 Å for $Cdc37_M$ and 0.8 Å for $Hsp90_N$ (0.5 Å for $Hsp90_N$ when excluding residues 106–127). The difference in the helical region (residues 106–127) of $Hsp90_N$ is due to the involvement of this region as a hydrophobic core in the complex structure.

Residue Leu-205 of Cdc37 Is Critical for the Complex Formation—Our structure of the $Hsp90_N$·$Cdc37_M$ complex indicates the important residues involved at the protein-protein interface. These residues can be divided into two categories: one forms typical salt bridge interactions, and the other forms the hydrophobic core of the complex as described previously. NMR cross-saturation transfer data show that Leu-205 in $Cdc37_M$ experiences the largest decrease in signal intensity. To assess the role of Leu-205, we mutated this residue to phenylalanine, isoleucine, alanine, glycine, aspartic acid, and glutamic acid. The two-dimensional ^1H,^{15}N-HSQC spectra of all mutants typically retain the spectra of the wild-type, except for the region around the mutation, indicating that there are no large conformational changes brought about by the mutation. Typically, NMR can identify protein-protein interactions even with as low affinity as ~5 mM (K_D). The wild-type $Cdc37_M$ binds to $Hsp90_N$ with a K_D of 4.0 μM (26, 32) and shows strong changes in the ^1H,^{15}N-HSQC spectrum upon complex formation. For mutants L205D and L205Q, changes in the ^1H,^{15}N-HSQC cannot be observed ([$Cdc37_M$]:[$Hsp90_N$] = 1:4), indicating that those $Cdc37_M$ mutants do not bind anymore to $Hsp90_N$ (Fig. 7). Control experiments showed that the L205F and L205I mutants retained the interaction, whereas there was a significant decrease in the affinity for mutants L205A and L205G. The observation supports that residue Leu-205 of $Cdc37_M$ drives the complex formation by its hydrophobic nature.

Comparison with Previously Published Yeast $Hsp90_N$-Human Cdc37 Crystal Structure—In our study we used human $Hsp90_N$, which has 69% sequence identity (Fig. 8) with that of the yeast homologue (32). However, the residues of Hsp90 in contact with Cdc37 are well conserved to a large extent, with the exception of Gln-123, which is serine in the case of yeast homologue. A superposition of our structure of the human $Cdc37_M$·$Hsp90_N$ complex with the Cdc37 (human)-Hsp90 (yeast) crystal structure (pdb: 1US7) (32) reveals a similar overall conformation, with an r.m.s.d. of 1.0 Å, when fitted onto the C_α atoms of the Cdc37. The interface of our NMR-based solution structure has a buried surface area of ~1600 Å^2, which is distinctly larger than the ~1100 Å^2 of the crystal structure. Our human $Cdc37_M$·$Hsp90_N$ structure is thus more compact than the previously reported heterogeneous structure. The most

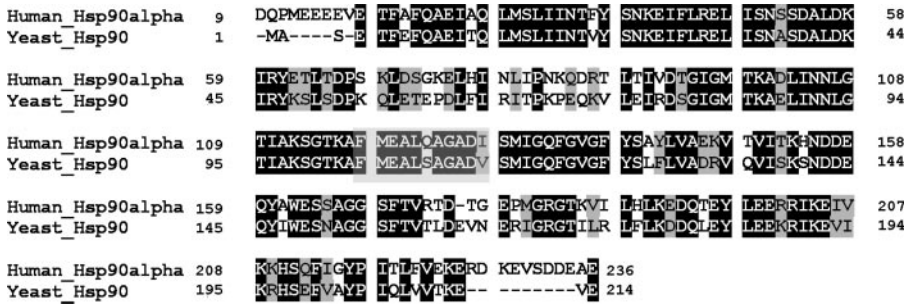

FIGURE 8. **Sequence alignment of human Hsp90$_N$ and yeast Hsp90$_N$.** The *shaded region* is the region that interacts with Cdc37$_M$ and forms the hydrophobic core of the interface.

eminent differences in Cdc37$_M$ are observed in the α_6-α_7-loop region. This difference already observed in the free-form crystal structure and very likely to arise from the fact that Cdc37 exists as a dimer in the crystal structure. Furthermore, changes are observed for the orientation of some side chains (Arg-167 and Gln-208) in the α_1-α_2 region of Cdc37$_M$.

DISCUSSION

Studying the protein-protein interaction of the full-length human Cdc37 (~45 kDa) with human Hsp90$_N$ (~23 kDa) at molecular detail by NMR is most challenging due to the relative large size of this complex. Because the best quality NMR spectra was obtained with the Cdc37$_M$ domain, which is known to interact with Hsp90, this study was focused on the examination of the Cdc37$_M$ structure and its interaction with Hsp90$_N$. An x-ray structure of human Cdc37$_M$ in complex with yeast Hsp90$_N$ was already available (32). In this study, an albeit longer Cdc37 construct (amino acids 148–347) was used. Interestingly, this construct was found to form a dimer. The core of the dimer interface has been reported to be around Gln-247 and Tyr-248 and the prolonged C terminus, which forms a small three-helix bundle (292–347), is not at all involved in dimer formation (32). However, we did not observe any evidence for dimer formation with the constructs used in our study. Also our experiments on the Cdc37$_M$·Hsp90$_N$ complex did not show signals that indicate formation of larger complexes. The existence of Cdc37$_M$ as a monomer was strongly supported by the high resolution x-ray structure of uncomplexed Cdc37$_M$ (Fig. 2). It should be noted, however, that the overall structure of monomeric and dimeric Cdc37$_M$ remains the same. The largest differences between the structures are found in the previously reported dimer interface, which is most probably caused by crystal packing and which is interestingly near to Hsp90 in the complex. Our findings for monomeric Cdc37 are also consistent with recent observations from Vaughan *et al.* (33) who analyzed a complex of Hsp90·Cdc37·Cdk4 by cryoelectron microscopy.

The interaction interface between human Cdc37$_M$ and Hsp90$_N$ was mapped based on NMR studies. Mapping of the CSPs and CSTs onto the structures reveals two eminent surface areas corresponding to a small area with charged residues and a large hydrophobic area. Subsequently, the docking program HADDOCK was used to calculate the NMR-based structure of the complex. When only using the ambiguous distance restraints that are based on all the existing data (CSPs, CSTs, and NOE) for the docking calculation, the final solutions did not converge and yielded two possible clusters with a different orientation. A single solution was obtained when we incorporated RDCs in our calculations. The overall conformation of the final NMR-based structure of the human complex is very similar to the known crystal structure of the heterogeneous complex. However, there are some clear differences observed for specific intermolecular contacts in the distinctly larger interaction interface, most probably causing this structure to be slightly more compact.

The Hsp90 residues in the interface of the complex are very well conserved, except for Gln-123, which is serine in case of the yeast homologue. In the crystal structure with the yeast homologue of Hsp90, this serine residue forms an intermolecular hydrogen bond with the Lys-202 side chain of Cdc37. In our model of the human complex, however, we find that the Gln-123 side chain is just outside the binding interface, and makes no significant contribution to the interaction. Instead, in this case, the nearby side chain of the Glu-120 residue of the human Hsp90 generally forms a hydrogen bond with the Lys-202 side chain of Cdc37. An important hydrogen bond is formed between Glu-47 (human sequence numbering) of Hsp90 and Arg-167 of Cdc37, which is considered to be the key interaction that arrests the ATPase action of Hsp90 (32). In the best structure from our docking bundle, we indeed also observe this hydrogen bond. However, we do not observe this hydrogen bond in all the docking structures, which is most probably a result of the two possible conformations for the side chain of Arg-167 that we observed in our free-form Cdc37$_M$ x-ray structure, that we use for our docking. We suppose that this side chain is flexible in the free-form Cdc37 and stabilizes the complex by forming an intermolecular hydrogen bond with Hsp90. Furthermore, in the heterogeneous crystal structure of the complex, the backbone oxygen of Hsp90 residue Gln-133 (human sequence numbering) accepts an intermolecular hydrogen bond from the side-chain Gln-208 of Cdc37, and its side-chain oxygen forms intermolecular hydrogen bonds with the backbone Arg-166 and Arg-167 amides of Cdc37. In our human complex we did not observe the interaction between the Hsp90 residue Gln-133 and the Cdc37 residue Gln-208. This could again be a result of the two possible conformations observed for this Gln-208 side chain we observed in the free-form x-ray structure, but on the other hand for the different orientation of this side chain in our human model, we observed that the amino moiety is rather close to the side-chain hydroxy of the Ser-113 residue of Hsp90, with which it may possibly form an intermolecular hydrogen bond. The hydrogen bonds between the side chain of Hsp90 residue Gln-133 and the backbone Arg-166 and Arg-167 amides of Cdc37 is very well maintained in our human structure of the complex. Furthermore, the hydrophobic core in our NMR-based structure of the com-

plex includes the proximity of Ala-124 of $Hsp90_N$ and Trp-193 of $Cdc37_M$, which are slightly further apart from each other in the heterogeneous crystal structure.

In recent years, the Hsp90 protein became attractive as a pharmaceutical anti-cancer target. Many protein kinases, of which some might be causative for cancer when deregulated or overexpressed, require Hsp90 to be maintained in a functional state. Targeting of Hsp90 thus seems to be attractive, because several protein kinases can be targeted at the same time. The Hsp90-specific inhibitor, 17-allylamino-17-demethoxy geldanamycin is already undergoing clinical trials (53). Hsp90-specific inhibitors known so far are directed against the ATP-binding pocket of Hsp90. Because Hsp90 needs co-chaperones to fulfill its function and one of these, Cdc37, is mainly found in combination with regulation of protein kinases, the whole Hsp90·Cdc37 complex could be considered as an interesting drug target. In addition, increased levels of Cdc37 have shown to enhance cancer cell growth (54). A drug that inhibits the formation of this complex might be a very valuable compound. Knowing the interaction interface of the Cdc37·Hsp90 is a prerequisite for designing substances inhibiting formation of the Hsp90·Cdc37. In our study we analyzed the human $Cdc37_M$·$Hsp90_N$ complex in great detail, and identified Leu-205 of Cdc37 as a key residue. This residue resides in the interface and makes many contacts with different residues of Hsp90 to stabilize the complex. Mutational analysis of Leu-205 indicates that the hydrophobic nature of this critical residue promotes the complex formation.

Very recently, a compound was identified that disrupts the Hsp90·Cdc37 complex in cancer cells (55) supporting the idea to target the Hsp90-Cdc37 interaction. We expect that the structure of the human $Cdc37_M$·$Hsp90_N$ complex solved in this study can be used to assist further studies in the development of small molecule inhibitors.

REFERENCES

1. Ferrarini, M., Heltai, S., Zocchi, M. R., and Rugarli, C. (1992) *Int. J. Cancer* **51,** 613–619
2. Yufu, Y., Nishimura, J., and Nawata, H. (1992) *Leuk. Res.* **16,** 597–605
3. Welch, W. J., and Feramisco, J. R. (1982) *J. Biol. Chem.* **257,** 14949–14959
4. Picard, D. (2002) *Cell. Mol. Life Sci.* **59,** 1640–1648
5. Terasawa, K., Minami, M., and Minami, Y. (2005) *J. Biochem.* (*Tokyo*) **137,** 443–447
6. Wegele, H., Mueller, L., and Buchner, J. (2004) *Rev. Physiol. Biochem. Pharmacol.* **151,** 1–44
7. Stebbins, C. E., Russo, A. A., Schneider, C., Rosen, N., Hartl, F. U., and Pavletich, N. P. (1997) *Cell* **89,** 239–250
8. Whitesell, L., and Lindquist, S. L. (2005) *Nat. Rev. Cancer* **5,** 761–772
9. Hunter, T., and Poon, R. Y. C. (1997) *Trends Cell Biol.* **7,** 157–161
10. MacLean, M., and Picard, D. (2003) *Cell Stress Chaperones* **8,** 114–119
11. Reed, S. I. (1980) *Genetics* **95,** 561–577
12. Reed, S. I., de Barros Lopes, M. A., Ferguson, J., Hadwiger, J. A., Ho, J. Y., Horwitz, R., Jones, C. A., Lorincz, A. T., Mendenhall, M. D., Peterson, T. A., Richardson, S. L., and Wittenberg, C. (1985) *Cold Spring Harbor Symp. Quant. Biol.* **50,** 627–634
13. Valay, J. G., Simon, M., Dubois, M. F., Bensaude, O., Facca, C., and Faye, G. (1995) *J. Mol. Biol.* **249,** 535–544
14. Whitelaw, M. L., Hutchison, K., and Perdew, G. H. (1991) *J. Biol. Chem.* **266,** 16436–16440
15. Brugge, J. S. (1986) *Curr. Top. Microbiol. Immunol.* **123,** 1–22
16. Mort-Bontemps-Soret, M., Facca, C., and Faye, G. (2002) *Mol. Genet. Genomics* **267,** 447–458
17. Basso, A. D., Solit, D. B., Chiosis, G., Giri, B., Tsichlis, P., and Rosen, N. (2002) *J. Biol. Chem.* **277,** 39858–39866
18. Lamphere, L., Fiore, F., Xu, X., Brizuela, L., Keezer, S., Sardet, C., Draetta, G. F., and Gyuris, J. (1997) *Oncogene* **14,** 1999–2004
19. Grammatikakis, N., Lin, J. H., Grammatikakis, A., Tsichlis, P. N., and Cochran, B. H. (1999) *Mol. Cell. Biol.* **19,** 1661–1672
20. Pearl, L. H. (2005) *Curr. Opin. Genet. Dev.* **15,** 55–61
21. Schwarze, S. R., Fu, V. X., and Jarrard, D. F. (2003) *Cancer Res.* **63,** 4614–4619
22. Stepanova, L., Yang, G., DeMayo, F., Wheeler, T. M., Finegold, M., Thompson, T. C., and Harper, J. W. (2000) *Oncogene* **19,** 2186–2193
23. Matts, R. L., and Caplan, A. J. (2007) in *Heat Shock Proteins in Cancer* (Calderwood, S. K., Sherman, M. Y., and Ciocca, D. R. eds.) 1st Ed., pp. 331–350, Springer Publishers, Dordrecht, The Netherlands
24. Siligardi, G., Panaretou, B., Meyerc, P., Singh, S., Woolfson, D. N., Piper, P. W., Pearl, L. H., and Prodromou, C. (2002) *J. Biol. Chem.* **277,** 20151–20159
25. Shao, J., Irwin, A., Hartson, S. D., and Matts, R. L. (2003) *Biochemistry* **42,** 12577–12588
26. Zhang, W., Hirshberg, M., McLaughlin, S. H., Lazar, G. A., Grossmann, J. G., Nielsen, P. R., Sobott, F., Robinson, C. V., Jackson, S. E., and Laue, E. D. (2004) *J. Mol. Biol.* **340,** 891–907
27. Lee, P., Rao, J., Fliss, A., Yang, E., Garrett, S., and Caplan, A. J. (2002) *J. Cell Biol.* **159,** 1051–1059
28. Scholz, G., Hartson, S. D., Cartledge, K., Hall, N., Shao, J., Dunn, A. R., and Matts, R. L. (2000) *Mol. Cell. Biol.* **20,** 6984–6995
29. Shao, J., Grammatikakis, N., Scroggins, B. T., Uma, S., Huang, W., Chen, J. J., Hartson, S. D., and Matts, R. L. (2001) *J. Biol. Chem.* **276,** 206–214
30. Shao, J., Prince, T., Hartson, S. D., and Matts, R. L. (2003) *J. Biol. Chem.* **278,** 38117–38120
31. Miyata, Y., and Nishida, E. (2004) *Mol. Cell. Biol.* **24,** 4065–4074
32. Roe, S. M., Ali, M. M. U., Meyer, P., Vaughan, C. K., Panaretou, B., Piper, P. W., Prodromou, C., and Pearl, L. H. (2004) *Cell* **116,** 87–98
33. Vaughan, C. K., Gohlke, U., Sobott, F., Good, V. M., Ali, M. M. U., Prodromou, C., Robinson, C. V., Saibil, H. R., and Pearl, L. H. (2006) *Mol. Cell* **23,** 697–707
34. Sreeramulu, S., Kumar, J., Richter, C., Vogtherr, M., Saxena, K., Langer, T., and Schwalbe, H. (2005) *J. Biomol. NMR* **32,** 262
35. Jacobs, D. M., Langer, T., Elshorst, B., Saxena, K., Fiebig, K. M., Vogtherr, M., and Schwalbe, H. (2006) *J. Biomol. NMR* **36,** 52
36. Dominguez, C., Boelens, R., and Bonvin, A. M. J. J. (2003) *J. Am. Chem. Soc.* **125,** 1731–1737
37. Muchmore, D. C., McIntosh, L. P., Russell, C. B., Anderson, D. E., and Dahlquist, F. W. (1989) *Methods Enzymol.* **177,** 44–73
38. Honig, B., Sharp, K., and Yang, A. S. (1993) *J. Phys. Chem.* **97,** 1101–1109
39. Keller, R. (2004) *The Computer Aided Resonance Assignment Tutorial, CANTINA*, Verlag, Goldau, Switzerland
40. Ottiger, M., Delaglio, F., and Bax, A. (1998) *J. Magn. Reson.* **131,** 373–378
41. Wang, Y. X., Marquardt, J. L., Wingfield, P., Stahl, S. J., Lee-Huang, S., Torchia, D., and Bax, A. (1998) *J. Am. Chem. Soc.* **120,** 7385–7386
42. Dosset, P., Hus, J. C., Marion, D., and Blackledge, M. (2001) *J. Biomol. NMR* **20,** 223–231
43. Zweckstetter, M., and Bax, A. (2000) *J. Am. Chem. Soc.* **122,** 3791–3792
44. Otwinowski, Z., and Minor, W. (1997) *Methods Enzymol.* **276,** 307–326
45. Collaborative Computation Project (1994) *Acta Crystallogr. D. Biol. Crystallogr.* **50,** 760–763
46. Navaza, J. (1994) *Acta Crystallogr. A.* **50,** 157–163
47. Murshudov, G. N., Vagin, A. A., and Dodson, E. J. (1997) *Acta Crystallogr. D. Biol. Crystallogr.* **53,** 240–255
48. Emsley, P., and Cowtan, K. (2004) *Acta Crystallogr. D. Biol. Crystallogr.* **60,** 2126–2132
49. Brunger, A. T., Adams, P. D., Clore, G. M., DeLano, W. L., Gros, P., Grosse-Kunstleve, R. W., Jiang, J. S., Kuszewski, J., Nilges, M., Pannu, N. S., Read, R. J., Rice, L. M., Simonson, T., and Warren, G. L. (1998) *Acta Crystallogr. D. Biol. Crystallogr.* **54,** 905–921
50. Linge, J. P., and Nilges, M. (1999) *J. Biomol. NMR* **13,** 51–59
51. Garcia, M. M., Jimenez Rios, M. A., and Garcia Bernal, J. M. (1990) *Int. J. Biol. Macromol.* **12,** 19–24

52. Lo Conte, L., Chothia, C., and Janin, J. (1999) *J. Mol. Biol.* **285,** 2177–2198
53. Ramanathan, R. K., Trump, D. L., Eiseman, J. L., Belani, C. P., Agarwala, S. S., Zuhowski, E. G., Lan, J., Potter, D. M., Ivy, S. P., Ramalingam, S., Brufsky, A. M., Wong, M. K. K., Tutchko, S., and Egorin, M. J. (2005) *Clin. Cancer Res.* **11,** 3385–3391
54. Gray, P. J., Jr., Prince, T., Cheng, J., Stevenson, M. A., and Calderwood, S. K. (2008) *Nat. Rev. Cancer* **8,** 491–495
55. Zhang, T., Hamza, A., Cao, X., Wang, B., Yu, S., Zhan, C. G., and Sun, D. (2008) *Mol. Cancer Ther.* **7,** 162–170
56. Kaelin, W. G., Jr. (2005) *Nat. Rev. Cancer* **5,** 689–698
57. Takahashi, H., Nakanishi, T., Kami, K., Arata, Y., and Shimada, I. (2000) *Nat. Struct. Biol.* **7,** 220–223